Journal of Ovarian Research

RESEARCH

Open Access

# A metabolic fingerprint of ovarian cancer: a novel diagnostic strategy employing plasma EV-based metabolomics and machine learning algorithms

Fei Long[2,3†], XingYu Pu[2,3†], Xin Wang[2,3†], DongXue Ma[2,3†], ShanHu Gao[2,3], Jun Shi[2,3], XiaoCui Zhong[1], Rui Ran[1], LianLian Wang[4], Zhu Chen[5], Yang Yang[6], Richard D. Cannon[7] and Ting-Li Han[1,2,3*]

## Abstract

Ovarian cancer (OC) is the third most common malignant tumor of women and is accompanied by an alteration of systemic metabolism. A liquid biopsy that captures and detects tumor-related biomarkers in body fluids has great potential for OC diagnosis. EVs, nanosized extracellular vesicles found in the blood, have been proposed as promising biomarkers for liquid biopsies. In this study we recruited 37 OC patients, 22 benign ovarian tumor (BE) patients, and 46 clinically healthy control patients (CON). Plasma EVs were purified from blood samples and sensitive thermal separation probe-based mass spectrometry analysis using a global untargeted metabolic profiling strategy was employed to characterize the metabolite fingerprints. Uniform manifold approximation and projection (UMAP) analysis demonstrated a distinct separation of EVs among the three groups. We screened for diagnostic biomarkers from plasma EV metabolites using seven machine learning algorithms, including artificial neural network (ANN), decision tree (DT), K nearest neighbor (KNN), logistics regression (LR), Naïve Bayes (NB), random forest (RF), and support vector machine (SVM). For the OC-CON comparison, the highest AUC values were found for RF (0.91), ANN (0.90) and NB (0.90), with the F1-scores of 0.88, 0.83, and 0.76 respectively. For the OC-BE comparison, SVM (0.94), RF (0.86), and KNN (0.86) gave the highest AUCs, with F1-scores of 0.80, 0.80, and 0.91 respectively. A total of 19 and 158 metabolic features exhibited significant differences (FC = 1.5, q < 0.01) in the OC vs BE and OC vs CON comparisons, respectively. Notably, the quantities of 9-octadecenamide and 1,4-methanobenzocyclodecene were significantly elevated, while maltol showed a significant reduction in the OC group compared to the BE group. When comparing the OC group to the CON group, the concentrations of 4-amino-furazan-3-carboxylic acid 2-hydroxy-4-methoxybenzaldehyde, N-phenylethyl, and 4-morpholineethanamine were significantly elevated, while the remaining metabolites, including hydrazine and pyridine sulfonamide, were reduced, in the OC group. The metabolites showing different abundancies are associated with cancer-related mutations, immune responses, and metabolic reprogramming. We demonstrate that the RF algorithm, combined with sensitive thermal separation probe-based mass spectrometry analysis of plasma EVs, can effectively identify OC patients with good accuracy. Thus, our study has shortlisted a set

†Fei Long, XingYu Pu, Xin Wang and DongXue Ma contributed equally to this work.

*Correspondence:
Ting-Li Han
tinglihan@cqmu.edu.cn
Full list of author information is available at the end of the article

of potential biomarkers in plasma EVs, and the proposed approach could serve as a routine prescreening tool for ovarian cancer.

**Keywords** Metabolomics, Machine learning, Metabolic pathways, Plasma, EVs, Ovarian cancer

## Introduction

### Ovarian cancer

According to the World Health Organization (WHO), in 2018, ovarian cancer (OC) ranked as the second most common malignancy among gynecological diseases, following cervical cancer, with an estimated 184,799 fatalities, which constitute approximately 6.6% of all cancer-related deaths. Due to its asymptomatic early stages [4], often OC is not diagnosed until it reaches an advanced stage, leading to a high fatality rate, earning it the moniker "silent killer" [25]. Indeed, OC is the deadliest malignant tumor of all female reproductive diseases [5]. Thus, it is necessary to understand the pathophysiology of OC and discover a more robust diagnostics tool. Liquid biopsy, as a non-invasive technique for cancer diagnosis, represents a novel and promising approach to cancer detection and monitoring [23].

### Extracellular vesicles (EVs)

The definitive diagnostic approach for cancer patients remains biopsies. Although there have been notable advances in the utilization of circulating tumor cells and circulating tumor DNA for diagnosing OC, issues remain for its early detection and disease progression monitoring [6]. Furthermore, the same issues apply to currently available clinical biomarkers. As a minimally invasive method, liquid biopsy offers the advantage of early diagnosis and real-time therapeutic response monitoring. This technique, which captures and detects tumor-related biomarkers in body fluids, shows significant promise for diagnostic application.

Extracellular vesicles (EVs), characterized by a phospholipid bilayer structure, are secreted by most cells and have potential as liquid biopsy biomarkers. They can be isolated from a variety of bodily fluids, including blood. Studies have revealed that the intracellular trafficking of EV cargo depends not only on the endocytic pathway but also on the biosynthetic secretory pathway for their release. This suggests that the contents of EVs can reflect the pathological and physiological states of the parental cells or source organs [18, 21, 26, 28]. EVs derived from OC tissue carry many tumor-related biomarkers, such as proteins, lipids, and nucleic acids, that are associated with disease progression. It has been demonstrated that EVs derived from OC patients' plasma exhibit higher concentrations of TGFβ1 and melanoma-associated antigen 3 (MAGE3) [17] than EVs from patients with benign disease, providing evidence of their potential as biomarkers for differentiating benign and malignant OC diseases. Furthermore, investigations have found an association of EV biomarkers with tumor stage and prognosis [20], indicating their potential roles in cancer diagnosis. Despite increasing research on OC EVs, there is a lack of studies investigating metabolomics-based biomarkers.

### The application of metabolomics to OC

Metabolic alterations occur downstream of genetic and proteomic regulation. Conversely, metabolic dysregulation can lead to gene overexpression or silencing [1], which ultimately impacts metabolites. Therefore, the metabolome, the most proximate phenotype among all 'omes', provides valuable insights into the biological responses to both internal and external perturbations, including growth, disease, genetic modifications, and environmental effects. In this context, analysis of metabolic patterns is an attractive strategy for monitoring dynamic changes in biological states.

Most studies use nuclear magnetic resonance (NMR) and gas or liquid chromatography combined with mass spectrometry (GC–MS or LC–MS) as analytical platforms for metabolic profiling. MS has higher sensitivity than NMR and is undoubtably the preferred choice for analyzing trace amounts of EV samples. GC exhibits a significant advantage over LC in terms of database completeness and is less prone to matrix effects and ion suppression by co-eluting compounds [10, 19], resulting in greater chromatographic resolution. However, there are some issues with the detection of polar, thermolabile, and non-volatile metabolites which require chemical derivatization prior to analysis [22]. The Agilent G4381A ChromatoProbe (a Thermal Separation Probe,TSP can be mounted on Agilent standard shunt/no-shunt or multi-mode injection ports in conjunction with the GC–MS system to quickly separate and identify metabolites in complex samples. This setup not only enables direct detection of metabolites but is also faster for scarce sample preparation and has higher sensitivity for trace metabolites, making it an effective solution for chemical derivatization.

Although there have been previous metabolomics studies on OC, there has been a lack of investigation of the EV metabolome related to OC. Therefore, we hypothesize that metabolites isolated from EVs in the blood of

OC patients can be utilized to differentiate these patients from healthy individuals. In the present study, we employed a sensitive TSP-based mass spectrometry analysis and combined it with machine learning algorithms to identify metabolite changes among plasma EVs obtained from OC patients, patients with benign ovarian tumor (BE) and clinically healthy control (CON) patients.

## Experimental section

### Study design and participants

The clinical study was conducted in accordance with the Declaration of Helsinki and approved by the Research Ethics Committee of the Second Affiliated Hospital of Chongqing Medical University (Chongqing, China). All participants were recruited from the Second Affiliated Hospital of Chongqing Medical University and provided informed consent prior to participation in the trial from July 2020 to December 2021. The patients were recruited according to the following inclusion and exclusion criteria: 1) Participants with severe chronic diseases such as hypertension, infectious disease, diabetes, metabolic disorders, or a diagnosis of malignancy other than ovarian cancer were excluded from this study to minimize recruitment bias; 2) the clinically healthy control patients ($n=46$) included women with uterine fibroids or endometrioma without any ovarian lesion; 3) the benign ovarian tumor group ($n=22$) included women with teratoma and ovarian cyst, and 4) the ovarian cancer group ($n=37$) were included based on levels of preoperative serum markers, including Carbohydrate Antigen (CA125 > 35 U/mL) and Human Epididymis Protein (HE4 > 70 pmol/L in pre-menopausal patients, or HE4 > 140 pmol/L in post-menopausal patients), and the imaging modality of sonography for evaluation of an adnexal mass. Details of the clinical samples and participants, including the age, BMI, tumor site, histological type, and stage of ovary cancer, are provided in Table 1.

### Blood collection

Peripheral blood samples (5 mL) were collected in EDTA tubes and delivered to the laboratory in an insulated ice box within 2 h. The samples were centrifuged at 1,000 g for 10 min to remove the blood cells and the supernatant plasma was stored at -80 °C until EV isolation.

**Table 1** Clinical characteristics of study participants

| Variable | Total ($N=105$) | Ovarian Cancer ($N=37$) | Benign ($N=22$) | Normal control ($N=46$) | *P* Value |
|---|---|---|---|---|---|
| **Age (years)** | | | | | < 0.001 |
| **N** | 105 | 37 | 22 | 46 | |
| **Mean ± SD** | 46.7 ± 13.8 | 53.4 ± 12.8 | 37.4 ± 11.7 | 41.2 ± 12.1 | |
| **Min–Max** | 18.0–74.0 | 20.0–74.0 | 20.0–70.0 | 18.0–68.0 | |
| **Median(Q1-Q3)** | 46.0(32.0–54.0) | 53.0(47.0–66.0) | 36.0(28.0–44.5) | 38.5(31.3–51.0) | |
| **BMI (kg/m$^2$)** | | | | | 0.618 |
| **N** | 105 | 37 | 22 | 46 | |
| **Mean ± SD** | 22.5 ± 2.9 | 22.2 ± 2.7 | 22.5 ± 2.4 | 22.8 ± 3.2 | |
| **Min–Max** | 16.0–30.0 | 17.5–27.9 | 18.4–28.2 | 16.0–30.0 | |
| **Median(Q1-Q3)** | 22.4(20.3–24.1) | 21.8(20.2–24.1) | 22.6(21.2–23.4) | 22.4(20.3–25.5) | |
| **OV** | | | | | |
| **Serous (%)** | 33(89.2) | 33(89.2) | N/A | N/A | |
| **Mucinous (%)** | 2(5.4) | 2(5.4) | N/A | N/A | |
| **Endometrioid (%)** | 1(2.7) | 1(2.7) | N/A | N/A | |
| **Others (%)** | 1(2.7) | 1(2.7) | N/A | N/A | |
| **FIGO stage** | | | N/A | N/A | |
| **IA(%)** | 1(2.7) | 1(2.7) | N/A | N/A | |
| **IC(%)** | 8(21.6) | 8(21.6) | N/A | N/A | |
| **IIB(%)** | 1(2.7) | 1(2.7) | N/A | N/A | |
| **III(%)** | 2(5.4) | 2(5.4) | N/A | N/A | |
| **IIIA(%)** | 2(5.4) | 2(5.4) | N/A | N/A | |
| **IIIC(%)** | 20(54) | 20(54) | N/A | N/A | |
| **IV(%)** | 2(5.4) | 2(5.4) | N/A | N/A | |
| **IVB(%)** | 1(2.7) | 1(2.7) | N/A | N/A | |

*P* value: significance was calculated by non-parametric Kruskal–Wallis H test, *OV* Ovary Cancer, *FIGO stage* stage of International Federation of Gynecology and Obstetrics, *N/A* No statistics are required for this variable

#### Isolation of EVs from plasma

To isolate the plasma EVs, we followed a modified differential ultracentrifugation method based on a previously described procedure [16]. PBS was filtered through a 0.22 μm PVDF filter before all EV isolation and characterization experiments. The resulting plasma samples were centrifuged at 5,000 g (4 °C) for 30 min to further eliminate cell debris. Next, the supernatant was diluted with PBS to a total of 12 mL and centrifuged at 100,000 g (4 °C) for 90 min to isolate total EV pellets, which were resuspended in 12 ml PBS for centrifugation again at 100,000 g (4 °C) for 90 min. The EVs were aliquoted and stored at -80℃ prior to verification of the isolated EVs and metabolomic analysis.

#### Transmission electron microscopy (TEM) analysis of EVs

Aliquots (4 μL) of EVs were dropped onto the carbon film copper grid and air-dried inside a fume hood overnight for TEM analysis to observe the morphology and ultrastructure of EVs. The grids were examined with a Hitachi-7500 transmission electron microscope (Hitachi, Tokyo, Japan) at an acceleration voltage of 80 kV.

#### Nanoparticle tracking analysis (NTA) of EVs

NTA analysis was performed to analyze the EV particle size and density distribution, as described previously [3]. Briefly, fresh EV samples (50 μL) were diluted in fresh phosphate-buffered saline (PBS) to a concentration between $1\times10^7$—$1\times10^9$ particles/mL, and vortexed for 1 min to resuspend aggregated pellets. The level of the camera capturing EVs videos with the NanoSight NS300 was set to 14. The optimal detection threshold was set to maximize the number of particles while ensuring that 10–100 red crosses were counted, with less than 10% not associated with distinct particles, and the blue cross count was restricted to 5. For each measurement, three 1-min runs were captured under the following conditions: cell temperature was maintained at 25 °C and the syringe speed was 40 μl/s. Then, the videos were analyzed using NanoSight NTA version 3.2 software (Malvern Panalytical Ltd., Malvern, UK). The resulting data were displayed in the form of a curve where the abscissa and the ordinate values represented the EV particle size and concentration respectively.

#### Western blot (WB) analysis of EVs

WB analysis followed a previously published method [16]. Briefly, portions (50 μL) of EV samples were lysed in lysis buffer (RIPA cracking solution, P0013B, Beyotime, China), with the addition of a protease inhibitor cocktail and PMSF. The released protein was centrifuged at 12,000 × g at 4℃ for 10 min, and then the supernatant was heated at 100℃ for 15 min with shaking. Primary antibodies were transferred onto the PVDF membrane (P0012A, Beyotime, China) from a 12% sodium dodecyl sulphate polyacrylamide gel (P0012A, Beyotime, China) and blocking with 8% BSA (4240GR005, Bio-Froxx, Germany), and the membrane was incubated at 4°C overnight. The primary antibodies used were CD63 (GR3212162-23, Abcam, 1:1000) and TSG101 (GR299332-32, Abcam, 1:5000). After washed with TBST solution three times, the membrane was incubated with horseradish peroxidase-conjugated secondary antibody (E030320, EARTHOX, USA) at room temperature for 1 h. Protein bands were visualized after electrophoretic separation with the GeneGnome XRQ analysis system (Syngene, UK).

#### Bicinchoninic acid (BCA) analysis

Protein concentration of EVs was measured with a BCA assay (P0012, Beyotime, China), and a protein standard curve according to the manufacturer's instructions, and used to adjust the loading concentration of EV samples for GC–MS analysis.

#### Thermal separation probe (TSP) and GC-inlet

The TSP (Agilent, US) extraction approach was implemented to measure trace amounts of metabolites in plasma EV samples with a single extraction step. EV samples (60 μL, $10^{8-10}$ particles per mL) were transferred to micro-vials (MicroV TSProbe Vial: 32 mm × 12 mm, Agilent, USA) and dried in a SpeedVac for 3 h. The micro-vials were inserted directly into the GC inlet with temperature programming (Multimode inlet, Agilent, USA) using the TSP apparatus.

#### Gas chromatography-mass spectrometry (GC–MS) analysis

An Agilent 5977A GC/MSD was used to detect trace metabolites in EV samples. Based on the resulting chromatogram, the GC resolution for the identified peaks ranged from 1 to 5,000. The GC-inlet was set at in the splitless mode with a flow rate of 1 mL/min helium carrier, and the inlet temperature initially at 120℃ and held for 6 s, then ramped the inlet temperature to 275℃ at a rate of 100 ℃. The volatile compounds were then separated on a DB-FFAP capillary column (30 m × 250 μm id × 0.25 μm, Agilent, CA, USA) and detected by mass spectrometry (Agilent 7890B-5977A) with electron impact ionization via electron emission at 70 eV. The GC–MS parameters were set following a previously published protocol [11]. The temperature was set at 250 °C, 230 °C, and 150 °C for the auxiliary, MS quadrupole, and

MS source respectively. The mass range was detected between 30 μm to 550 μm in trace ion detection mode, the threshold was 150, and the scan speed was set at 2.8 scans/sec. The oven temperature program was as follows: (1) 70 °C hold for 2 min; (2) increase to 150 °C at 50 °C/min then hold for 3 min; (3) increase to 190 °C at 15 °C/min then hold for 5 min; and (4) reach 240 °C at 20 °C/min then hold for 5 min. The whole process took 21.77 min.

#### Quality control

To minimize the batch variability, an equal volume of EVs derived from the plasma from the OC, BE, and CON groups was pooled together to prepare the quality control (QC) samples, and blank samples comprised empty micro-vials solely containing an internal standard. For each sample batch analysis, the first three samples analyzed were blanks, and then the QC samples were incorporated as the first, middle, and last EV sample for the GC–MS batch.

#### Metabolite identification, quantification and normalization

The chromatographic peaks were deconvoluted and identified using Automated Mass Spectral Deconvolution & Identification System software. The metabolites were identified if they matched both the in-house MFC library spectra > 90% and their respective GC retention time within a 30-s window. The identification of remaining compounds used a commercial NIST mass spectral library.

The relative concentration of metabolites was calculated using the MassOmics R-based script from the peak height of the most abundant fragmented iron mass within a predetermined retention time. The background contamination and any carryover from the previous analysis was subtracted using blank samples. The relative concentration of identified compounds was first normalized to the internal standard (d4-alanine). Median centering of QC samples was implemented to adjust for batch effects. Dilution correction was achieved using the albumen concentration measured with the BCA assay.

#### Machine learning development and classification

Since different machine learning models may predict or rank different classification results, seven machine learning methods were performed to build the most appropriate binary classifier for identifying the category of samples. Classifiers included artificial neural network (ANN), decision tree (DT), K nearest neighbor (KNN), logistics regression (LR), Naïve Bayes (NB), random forest (RF), and support vector machine (SVM). First, identified metabolites were corrected with a data rectification procedure encompassing standard internal, QC samples, and protein concentration. Subsequently, the metabolite data were randomly split into the training and testing datasets in a ratio of 75:25 by Stratified Random Sampling. Each dataset was scaled independently by a z-score normalization algorithm to rescale each metabolite feature. According to the feature importance information, the significant features subset was selected by the random forest-recursive feature elimination algorithm (RF-RFE) method with the training dataset. The seven supervised machine learning models with the selected metabolite features were trained to build efficient classifiers using the R-library packages, including Caret (v6.0–90), neuralnet (v1.44.2), e1071 (v1.7–9), kknn (v1.3.1), and C50 (v0.1.5). The hyper-parameter settings are shown in Table 2. To further validate the model, the validation dataset was employed to evaluate model performance. Confusion matrix and receiver operator characteristic (ROC) curves were used to evaluate the performance of classifiers and provided a calculating foundation of metrics including accuracy, recall (sensitivity), specificity, precision (positive predictive value), negative predictive value, and F1 value, which were defined as follows:

$$\text{Accuracy} = (TP + TN)/(TP + FP + TN + FN);$$

$$\text{Recall} = TP/(TP + FN);$$

$$\text{Specificity} = TN/(TN + FP);$$

$$\text{Precision} = TP/(TP + FP);$$

$$\text{Negative predictive value} = TN/(TN + FN);$$

$$F1 = 2 * (\text{Precision} * \text{Recall})/(\text{Precision} + \text{Recall}).$$

TP, true positive; TN, true negative; FP, false positive; FN, false negative.

#### Overall experimental design of this study

A schematic diagram of the study approaches and main findings is presented in Fig. 1. Plasma EVs were purified from blood samples obtained from both ovarian cancer (OC) patients and non-malignant patients using ultracentrifugation. The global untargeted metabolite fingerprint of plasma-derived EVs was characterized using a sensitive thermal separation probe (TSP)-based mass

**Table 2** The hyper-parameter settings of the machine learning models

| Models | Parameters | Parameter ranges | Optimal parameters |
|---|---|---|---|
| ANN | hidden;<br>linear.output | hidden:c(1,1,1) ~ c(10,10,10);<br>linear.output:FALSE;<br>learningrate: 0.001 ~ 0.050 | hidden = c(10,7,4);<br>linear.output = FALSE<br>learningrate = 0.013 |
| DT | method;<br>metric;<br>trControl<br>tuneGrid | method: "C5.0";<br>metric: "ROC";<br>trControl: trainControl(method = "cv",<br>selectionFunction = "oneSE")<br>tuneGrid* = expand.grid(.model = "tree",.trials = c(1,2,3,4,5,<br>6,7,8,9,10,11,12,13,14,15,16,17,18,19,20,21,23,24,25,<br>26,27,28,29,30,31,32,33,34,35,36,37,38,39,40)) | method = "C5.0";<br>metric = "ROC";<br>trControl = trainControl(method = "cv",selectionFunction = "oneSE")<br>tuneGrid* = expand.grid(.model = "tree",.trials = c(1,2,3,4,5,6,7,8,9,10,<br>11,12,13,14,15,16,17,18,19,20,21,23,24,25,26,27,28,29,30,31,32,33,<br>34,35,36,37,38,39,40)) |
| KNN | kernel | Kernel: "triweight";<br>k: 1 ~ 30;<br>d: 1 ~ 10 | kernel = "triweight";<br>k = 15;<br>d = 2 |
| LR | maxit | maxit: 1 ~ 100 | maxit = 50 |
| NB | - | - | - |
| RF | method;<br>selectionFunction;<br>metric;<br>trControl | method: "rf";<br>selectionFunction: "oneSE";<br>metric: "Kappa";<br>trControl:trainControl(method = "cv",selection<br>Function = "oneSE") | method = "rf";<br>selectionFunction = "oneSE";<br>metric = "Kappa";<br>trControl = trainControl(method = "cv",selectionFunction = "oneSE") |
| SVM | method;<br>tuneLength;<br>trControl | method: "svmRadial";<br>tuneLength: 1 ~ 50;<br>trControl:trainControl(method = "cv", selection<br>Function = "oneSE") | method = "svmRadial";<br>tuneLength = 12;<br>trControl = trainControl(method = "cv",selection<br>Function = "oneSE",classProbs = TRUE) |

- parameters were set as default * the optimal value was automatically tuned by R software

spectrometry analysis. To screen potential diagnostic biomarkers for ovarian cancer, we employed seven machine learning algorithms, namely Artificial Neural Network (ANN), Decision Tree (DT), k-Nearest Neighbors (KNN), Logistic Regression (LR), Naive Bayes (NB), Random Forest (RF), and Support Vector Machine (SVM). Together with the integration of machine learning modelling, this enabled us to pinpoint plasma EV metabolites intricately related to various cancer phenotypes, encompassing cancer-related mutations, immune responses, and metabolic reprogramming.

### Statistical analysis

The non-parametric Kruskal–Wallis H test was performed to evaluate the differences in the clinical characteristics of three groups: OC, BE, and CON patients. Uniform manifold approximation and projection (UMAP) was plotted to illustrate the overall relationship between the three groups using the UMAP R-package. The ROC curve was implemented to determine the predictability of the classifier using the POCR R-package. The Upset diagram and heatmap were constructed using UpSetR and ggplot2 R-packages respectively. Our Pathway Activity Profiling (PAPi) algorithm was used to predict and compare the relative activity of different metabolic pathways in the OC group and the CON group based on metabolite profiling results. This programme connects to the KEGG online database (http://www.kegg.com) and uses the number of metabolites identified from each pathway and their relative abundances to predict which metabolic pathway is likely to be active in the EV, and chord plots connecting metabolites and their participating metabolic pathways were reconstructed via the GOplot R-package. Significant differences in metabolic pathway activities were determined by $P$-values < 0.05 and corresponding FDR values < 0.2 using the q-value R-package.

### Ethical approval

The clinical study was conducted in accordance with the Declaration of Helsinki. The studies involving human participants were reviewed and approved by the Research Ethics Committee of the Second Affiliated Hospital of Chongqing Medical University, China (202,164). The participants provided their written informed consent to participate in this study.

## Results and discussion

### Clinical characteristics of study participants

Plasma EVs obtained from participants with ovarian cancer (OC, $n = 37$), benign tumor (BE, $n = 22$), and clinically healthy control patients (CON, $n = 46$) were isolated in order to identify potential biomarker candidates. The clinical characteristics of the patients are summarized in Table 1. The $P$-value for age was less than 0.001, indicating

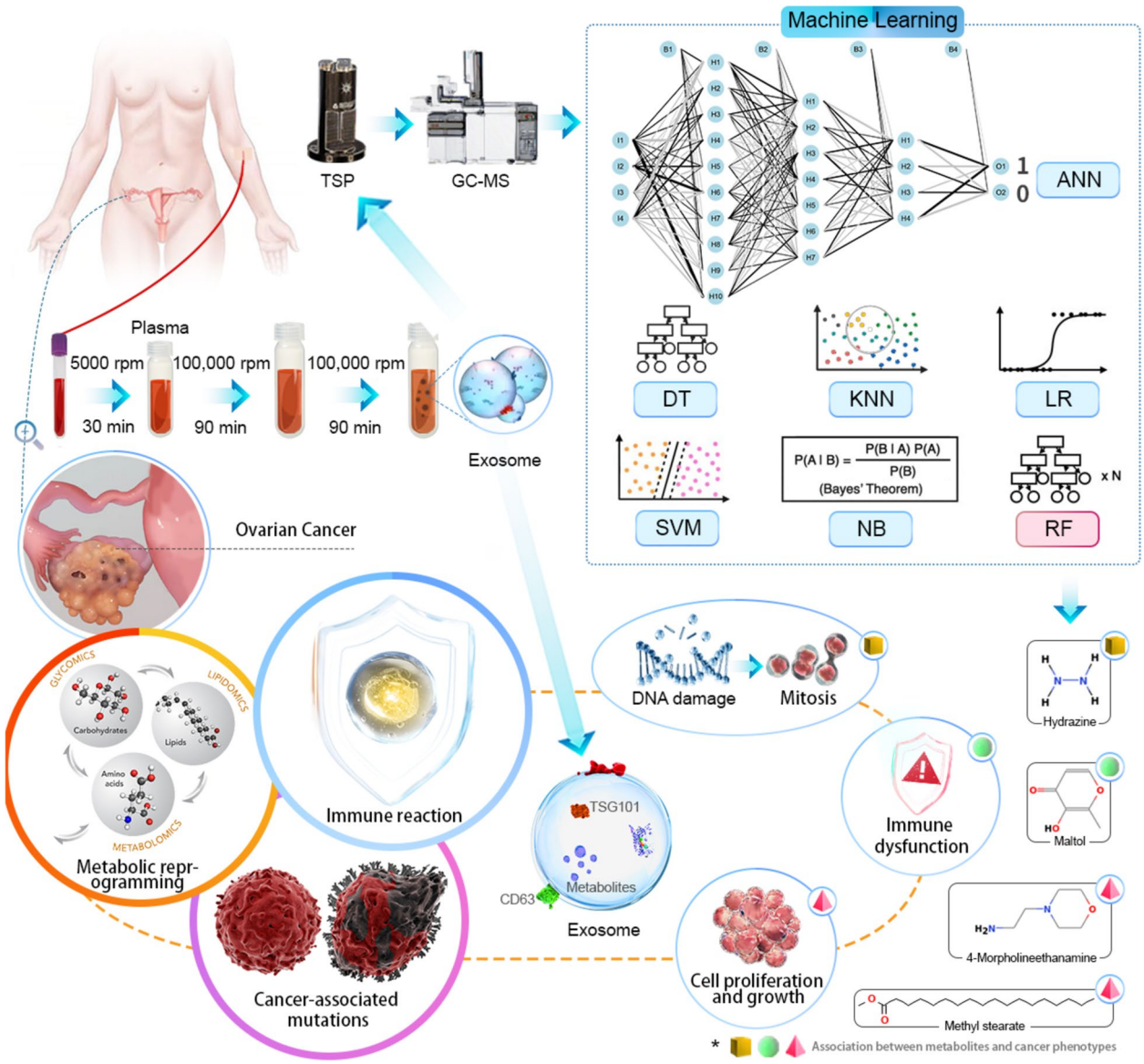


**Fig. 1** Schematic diagram of study approaches and main findings. RF model combined with TSP mass spectrometry analysis of plasma EVs demonstrated a remarkable capability to identify OC patients accurately. Notably, metabolites contributing to this discrimination included hydrazine, maltol, 4-morpholineethanamine, and methyl stearate. These identified metabolites are associated with cancer phenotypes, such as cancer-related mutations, immune responses, and metabolic reprogramming

a statistically significant age difference among the participant groups. Conversely, there was no statistically significant difference in terms of BMI (*P*-value = 0.618). The majority of OC cases (89.2%) were classified as high-grade serous. Among patients with malignant tumors, there were 9, 1, 24, and 3 patients in stages I, II, II, and IV respectively.

### Isolation and evolution of EVs

The EVs derived from the OC, BE, and CON participants were isolated from 5 mL of plasma using differential ultracentrifugation. TEM, NTA and western blotting were used to validate the quality of the isolated EVs from plasma (Fig. 2). TEM showed that the vesicles were spherical membrane structure with a size range of 50–150 nm (Fig. 2A). In addition, the NTA size distribution showed that the median diameter of EVs was 126.5 nm (range: 100—500 nm), which is consistent with other studies [7] (Fig. 2B). The NTA also revealed a nanoparticle concentration of $1.45 \times 10^9$ particles/mL. Based on the formula below, the derived from OC tissue concentration of EVs in the original plasma sample was estimated to be $1.16 \times 10^9$ EVs/mL.

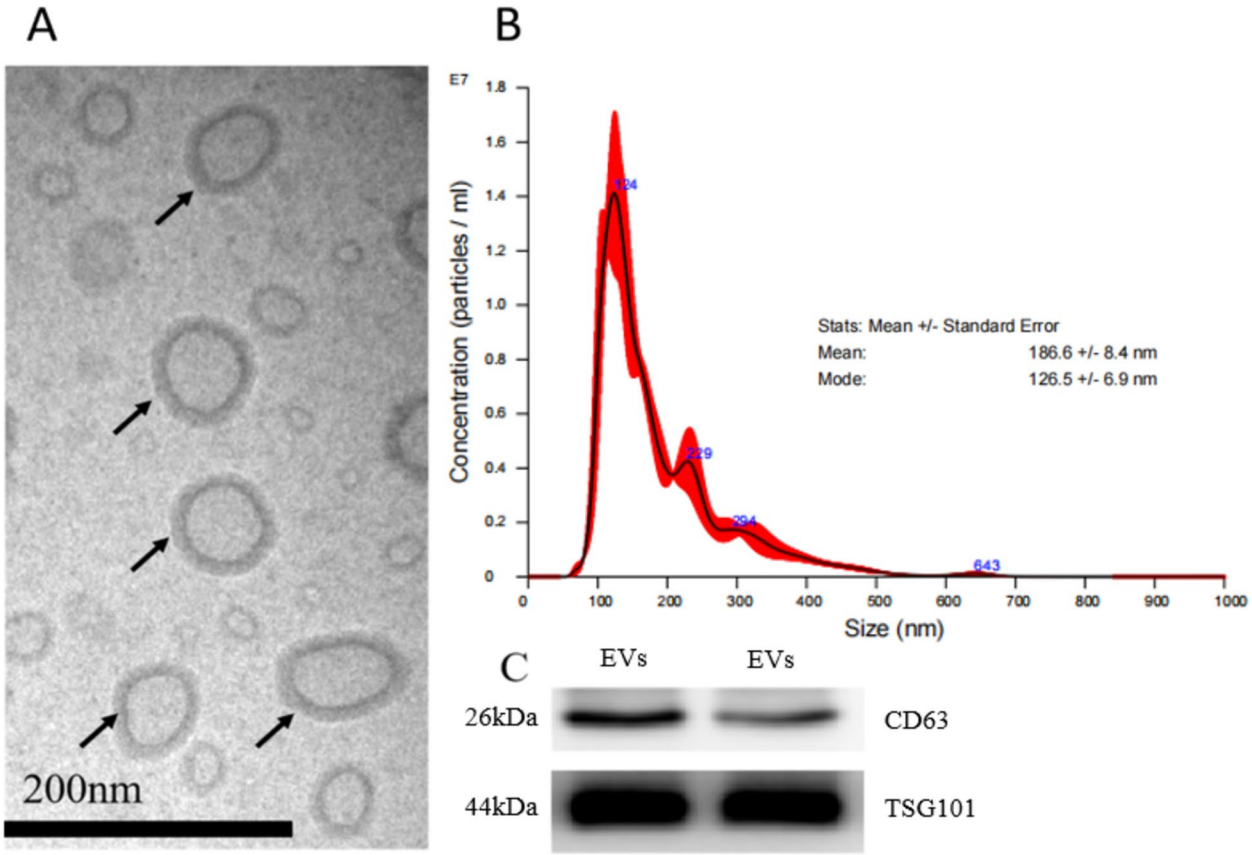


**Fig. 2** The characterization of EVs. **A** Representative electron microscopy micrograph of EVs isolated from plasma (indicated by arrows), bar = 200 nm. **B** NTA analysis to determine the size distribution and number of EVs. **C** Western blotting validated EVs through CD63 and TSG101

$$\text{Final exosomes concentration} = \frac{\text{NTA result}}{\text{exosome size of each detected NTA sample}} \times \frac{\text{exosome size of each plasma sample}}{\text{plasma sample size}} = \frac{1.45 \times 10^9}{50\mu\text{L}} \times \frac{200\mu\text{L}}{5\text{mL}} = 1.16 \times 10^9/\text{mL}$$

The membrane proteins CD63 and TSG101 (common EV markers) were highly enriched in EVs from patients detected by western blotting (Fig. 2C). Due to the utilization of all EV samples from the plasma of OC patients, analysis of negative EV markers such as GM130 and GRP94 was not performed in the WB experiment.

### Overall changes in metabolite profiles

Alterations in cellular metabolism have been reported in numerous human cancers and are thought to reflect the metabolic demands related to cancer development [29]. In this study we performed comprehensive metabolic profiling of plasma EV samples collected from 105 women diagnosed either with OC, BE, or CON. Uniform manifold approximation and projection (UMAP) was employed utilizing 388 chromatographic peaks identified in EVs. The results demonstrated a distinct separation of EVs among the three groups, as depicted in Fig. 3A. Furthermore, we undertook pairwise comparisons of the metabolite profiles detected in the OC, BE, and CON groups. A total of 19 and 158 metabolites exhibited significant differences in abundance (FC = 1.5, $q < 0.01$) in the comparisons between OC vs BE and OC vs CON, respectively (Fig. 3B). These differences were visualized through a heat map and volcano plots in Fig. 4A-C. In the comparison between the OC and BE groups, the quantities of 9-octadecenamide and 1,4-methanobenzocyclodecene were significantly elevated in OC group, while maltol showed a significant reduction. The concentrations of 4-amino-furazan-3-carboxylic acid 2-hydroxy-4-methoxybenzaldehyde, N-phenylethyl, and 4-morpholineethanamine were significantly higher in the OC group than in the CON group, while the remaining metabolites, including hydrazine and pyridine sulfonamide, were lower. Several of the identified metabolites have been previously implicated in cancer pathogenesis. For instance, Spencer and Kisby demonstrated that

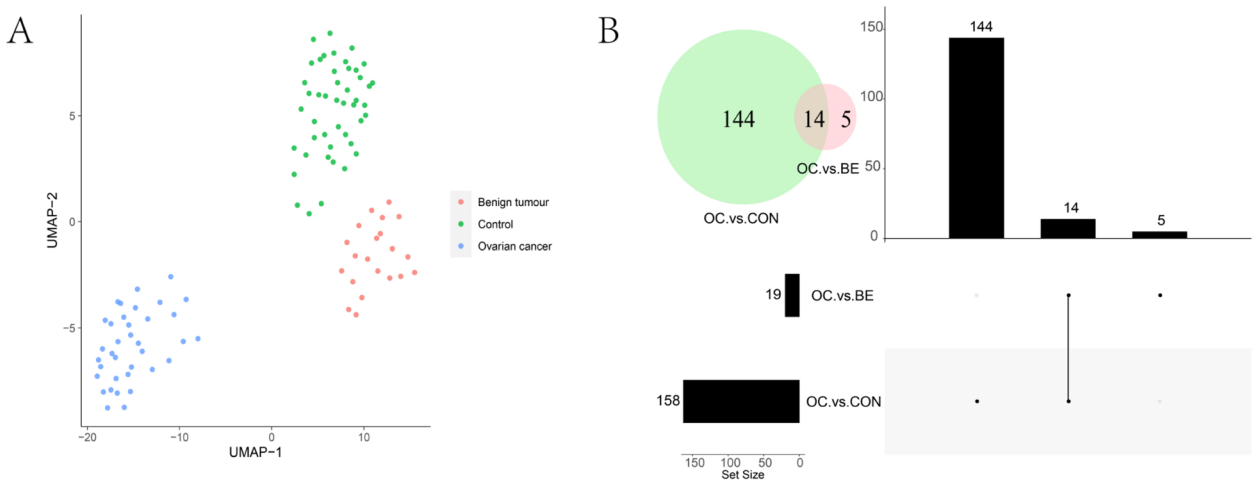


**Fig. 3** UMAP, Upset plot, and Venn diagram of EV samples from study participants. **A** UMAP clustering of all participant samples colored according to the participant group; each point in the plot represents a participant. Red dots represent the benign tumor group ($n = 22$), green dots indicate the control group ($n = 46$), and blue dots represent samples derived from the ovarian cancer group ($n = 39$). **B** Upset plot and Venn diagram of metabolites with differential abundance ($p < 0.05$). The individual or connected dots represent the various intersections of metabolites that were either unique to, or shared among, comparisons

hydrazine induces DNA damage, which consequently leads to mutations and unregulated mitosis [24]. Similarly, another study reported that maltol substantially inhibited tumor growth through the enhancement of immune function, induction of apoptosis, and inhibition of angiogenesis [14]. Our findings are consistent with those of Bachmayr et al. [2], who observed alterations in the blood metabolites of OC patients; specifically, reductions in lipids and amino acids were directly associated with tumor metabolism and facilitated cellular proliferation and growth [2]. Collectively, these metabolites showing differential abundancies are linked to cancer-related mutations, immune responses, and metabolic reprogramming, thus indicating their potential utility as diagnostic biomarkers for OC.

#### Metabolic pathway enrichment analysis

To gain further insights into the biological role of the identified metabolites, we conducted a pathway enrichment analysis using the KEGG metabolic network database (Fig. 5A). The results of the predicted pathway analysis revealed that only the butanoate metabolism pathway was upregulated in EVs derived from the OC group. In contrast, nearly all other metabolic pathways, including carbohydrate metabolism, lipid amino acid metabolism, cofactor metabolism, vitamin metabolism, and xenobiotic biodegradation, were found to be downregulated in the OC group. Furthermore, the metabolites with differential abundance were then mapped to 17 significant metabolic pathways including glycolysis, gluconeogenesis, and the metabolism of glyoxylate, dicarboxylate, butanoate, glutathione, glycerophospholipid, pyruvate, glycine, serine, threonine, tyrosine, phenylalanine, tryptophan, nicotinate, nicotinamide, propanoate, ubiquinone, and bile acids as illustrated by the Sankey diagram in Fig. 5B. Other studies have found similar metabolic alterations in OC. For example, Zhong et al. observed an upregulation of glutathione metabolism in women diagnosed with this malignancy [29]. Elevated glutathione metabolism has been shown to accompany tumor growth, presumably to counteract the increased oxidative stress arising from accelerated metabolic rates [9, 12, 29]. In addition, Denkert et al. revealed elevated levels of amino acid intermediates, such as glycine, in OC tissues [8]. The increase in amino acid metabolism suggests that substantial pools of intermediate nutrients are being mobilized for molecular assembly in cancer cells. Research by Xu et al. demonstrated that butyrate promotes cancer cell apoptosis by acting as a SIRT3 inhibitor. The authors showed that butyrate-induced acetylation of Pyruvate Dehydrogenase E1 Subunit Alpha 1 (PDHA1) alleviated the inhibitory phosphorylation of PDHA1 at serine 293, thereby facilitating the flow of glycolytic intermediates into the tricarboxylic acid (TCA) cycle and reversing the Warburg effect. Meanwhile, high levels of acetylation induced by butyrate inactivated complex I of the electron transport chain, preventing its use as an intermediate in the TCA cycle. These metabolic stresses promote apoptosis in high-glucose cancer cells. The findings reported by Xu et al. further support the upregulation of butyrate observed in the OC group in this study. In conclusion,

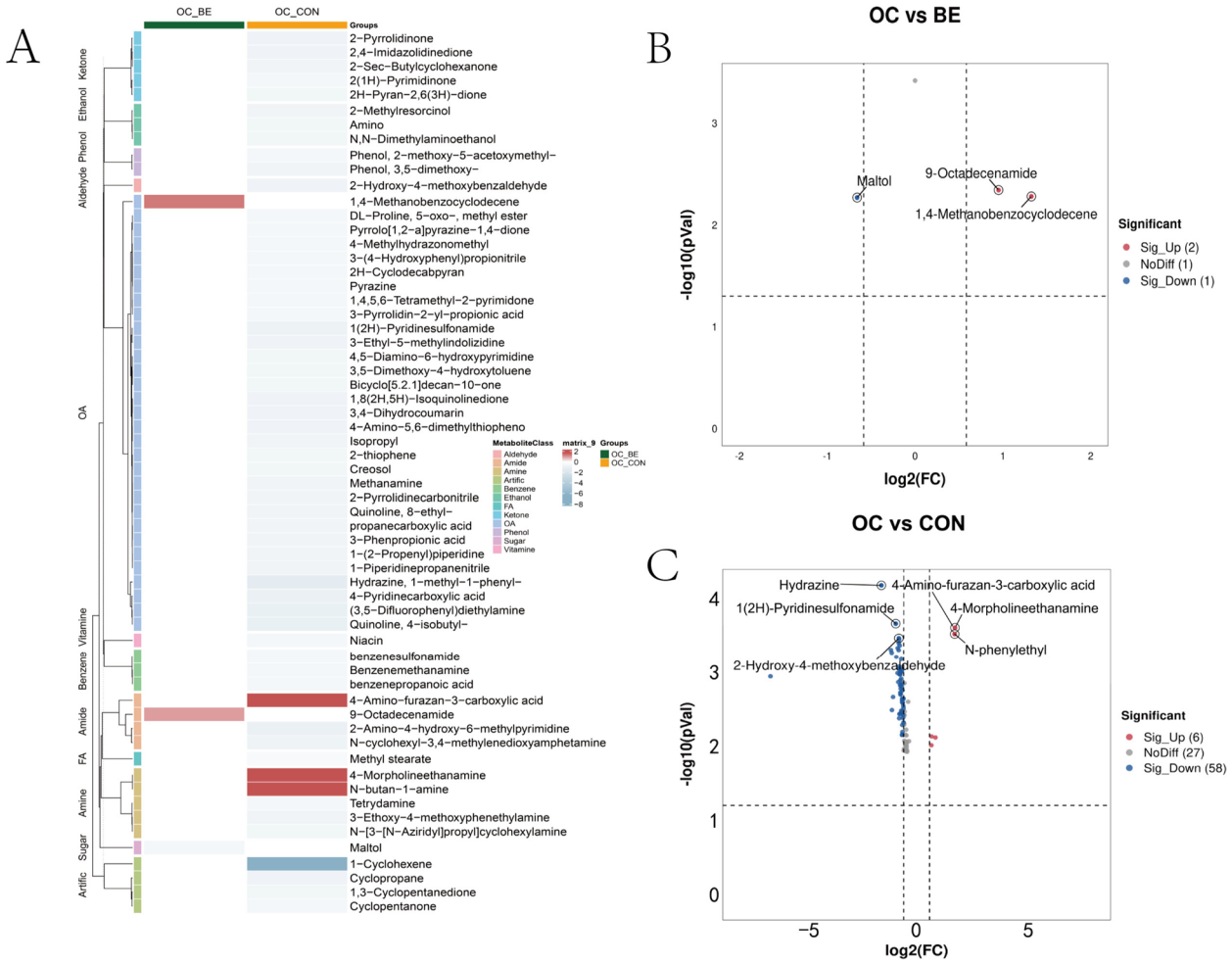


**Fig. 4** Metabolite profiles of the EV samples from study participants. **A** Heat Map showing the profile of metabolites in plasma EV samples and their metabolic classifications. The relative concentration of metabolites in the samples are expressed on a $\log_2$ scale. The red block indicates that the metabolite level in the divisor array is higher than that in the divisor array, while the blue block indicates that the metabolite level in the divisor array is lower than that in the divisor array. Only metabolites with both *p*-value and q-value less than 0.01 in the logistic regression adjusted for age and BMI are displayed. **B**<**C** Volcano plot of the metabolites with differential abundance ($p < 0.05$, FC > 1.5). Red dots indicate upregulation and blue dots indicate downregulation

this research provides novel insight into the metabolite phenotype of plasma EVs that discriminates OC from BE and normal ovarian pathophysiology.

### Machine learning algorithms for disease prediction

In order to determine which metabolites can be used to discriminate the OC group from the BE and CON groups, we used binary classification algorithms including artificial neural network (ANN), decision tree (DT), K nearest neighbor (KNN), logistics regression (LR), Naïve Bayes (NB), random forest (RF), and support vector machine (SVM). Prior to modelling for the OC-BE and the OC-CON comparison groups with 59 and 83 samples respectively, each group was shuffled randomly. To avoid overfitting, the model was built using split data, 60% of the training and 20% of the test set and validation set.

As a result of applying these the algorithms to the dataset, a panel of metabolites in the plasma EVs was identified from 388 features. This included 1,4-methanobenzocyclodecene, 9-octadecenamide, methyl stearate, 4-morpholineethanamine, decanoic acid, aminophenylacetylene, lacthydrazide, pentanone, 2,4-ditert butylphenol, phenol, 3,5-dimethoxy, phenpropionic acid and silacyclopentane. The contributions of the nominated metabolites to the performance of each machine learning algorithm were ranked (Supplementary Fig. 1). The area under the curve (AUC) of biomarker signatures discriminating the OC from the CON and BE groups are

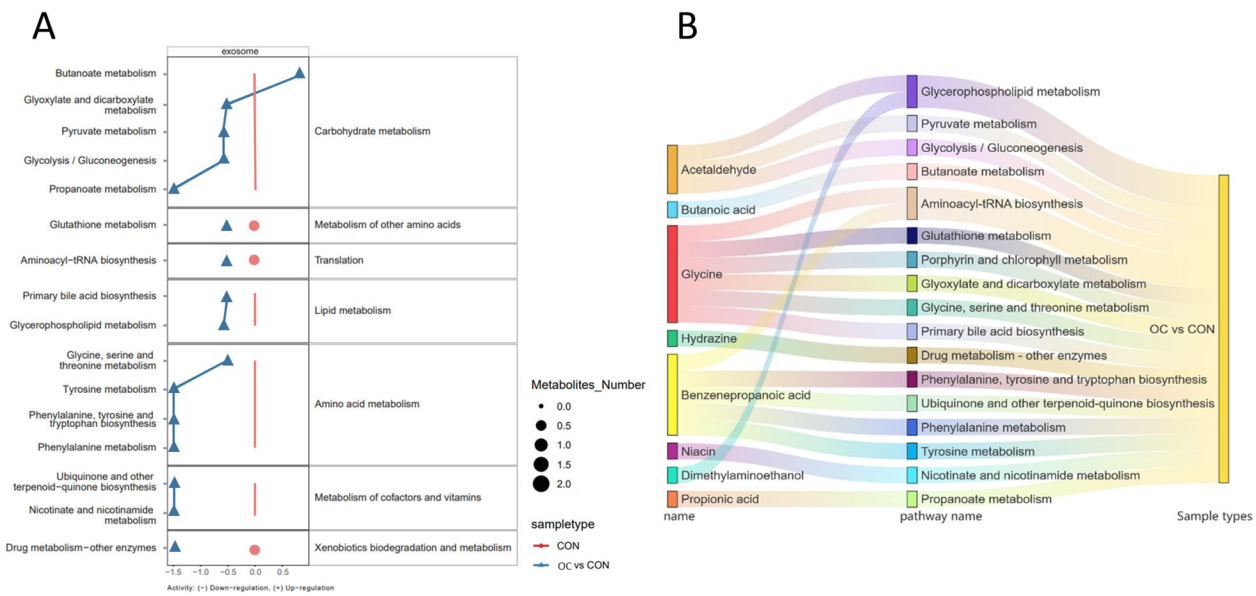


**Fig. 5** Different metabolic pathways and metabolic networks in ovarian cancer (OC) and clinically healthy control patients (CON) groups. **A** Activities of metabolic pathways in EVs derived from the plasma of the OC and CON groups. Red dots and lines represent the metabolic activities in EVs from the CON group that were adjusted to 0. Blue triangles represent metabolic activities in EVs from the OC group relative to the CON group. The metabolic activities are expressed on a $\log_2$ scale. The triangle size indicates the number of identified metabolites in the pathway. Only the metabolic pathways with a significant *p*-value less than 0.01 (Logistic regression with age as a confounding factor) are plotted. **B** A Sankey diagram displaying how the metabolites with differential abundance connect to their participating metabolic pathways

**Table 3** Performance of 7 machine learning models

| | **Algorithms** | | | | | | |
|---|---|---|---|---|---|---|---|
| | RF | ANN | NB | KNN | SVM | DT | LR |
| **OC vs CON** | | | | | | | |
| AUC | 0.91 | 0.90 | 0.90 | 0.87 | 0.88 | 0.80 | 0.61 |
| Sensitivity | 0.92 | 0.83 | 0.67 | 0.75 | 0.67 | 0.67 | 0.58 |
| Specificity | 0.78 | 0.78 | 0.89 | 0.78 | 0.78 | 0.78 | 0.56 |
| PPV | 0.85 | 0.83 | 0.89 | 0.82 | 0.80 | 0.80 | 0.64 |
| NPV | 0.88 | 0.78 | 0.67 | 0.70 | 0.64 | 0.64 | 0.50 |
| Precision | 0.85 | 0.83 | 0.89 | 0.82 | 0.80 | 0.80 | 0.64 |
| F1 | 0.88 | 0.83 | 0.76 | 0.78 | 0.73 | 0.73 | 0.61 |
| **OC vs BE** | | | | | | | |
| AUC | 0.86 | 0.80 | 0.83 | 0.86 | 0.94 | 0.69 | 0.73 |
| Sensitivity | 0.80 | 0.60 | 0.80 | 1.00 | 0.80 | 0.80 | 0.80 |
| Specificity | 0.86 | 0.86 | 0.71 | 0.86 | 0.86 | 0.57 | 0.71 |
| PPV | 0.80 | 0.75 | 0.67 | 0.83 | 0.80 | 0.57 | 0.67 |
| NPV | 0.86 | 0.75 | 0.83 | 1.00 | 0.86 | 0.80 | 0.83 |
| Precision | 0.80 | 0.75 | 0.67 | 0.83 | 0.80 | 0.57 | 0.67 |
| F1 | 0.80 | 0.67 | 0.73 | 0.91 | 0.80 | 0.67 | 0.73 |

displayed in Table 3. RF (0.91), and ANN (0.90) and NB (0.90) resulted in the highest AUC values with F1-scores of 0.88, 0.83, and 0.76, respectively, for the OC-CON comparison. Meanwhile, for the OC-CON comparison, the RF classifier displayed the best discrimination power (AUC value of 0.91) based on the top-ranking features. For the OC-BE comparison, SVM (0.94), RF (0.86), and KNN (0.86) gave the highest AUC values with F1-scores of 0.80, 0.80, and 0.91, respectively. To further assess the performance of the top-ranking features, an independent

plasma EV dataset ($n=29$) was recruited to validate the models. We observed that the external validation of the independent EV dataset yielded AUC values of 0.86 (RF and SVM) and 0.91 (KNN and SVM) for the OC-BE and OC-CON comparisons, respectively (Supplementary Table 1). Notably, RF provided the overall best performance for both model tests and the validation because it is a machine-learning approach for binary classification and can handle smaller datasets well [27]. DT and LR appeared to give the worst performance, likely due to underfitting resulting from a smaller dataset [13]. Considering the pros and cons of the different machine learning algorithms (Supplementary Table 2), we determined that RF was an appropriate model for our relatively small dataset and binary research question.

Despite the promising discriminative power of RF model for distinguishing between the OC and CON/BE groups, the identified top-ranking signatures, including 4-morpholineethanamine (100), maltol (100), 4-Aminofurazan-3-carboxylic acid (89), and bicyclo[5.2.1] decan-10-one (87) have not previously been reported as diagnostic biomarkers for OC. For example, Zhong et al. have shortlisted several metabolites, such as succinic acid, lactic acid, itaconic acid, malic acid, glutamic acid and glutathione, as potential biomarkers for OC in plasma and urine [29]. Liu et al. conducted a screening of nine differential metabolites from 37 OC tissues and their ascites [15]. The metabolites were 20-COOH-leukotriene E4, 1,25-dihydroxyvitamin D3-26,23-lactone, 20a,22b-dihydroxycholesterol, 3a,6a,7b-trihydroxy-5b-cholicacid, and 3a,7a,12a,19-tetrahydroxy-5b-cholic acid [15]. We have identified different diagnostic metabolites. One possible reason for this discrepancy is that our study primarily focused on plasma EVs, while other research predominantly employed conventional biological specimens such as tissue, plasma, hair, and ascites. Furthermore, in order to investigate the trace metabolite concentrations within plasma EVs, we employed a novel TSP. This probe enabled direct analysis of metabolites without sample preparation, which is superior to the conventional method of organic liquid extraction used for mass spectrometry analysis.

Despite the promising results, several limitations of our research merit discussion. Firstly, the ovaries are situated deep within the pelvic cavity, and early-stage ovarian lesions often present with non-specific clinical symptoms. By the time symptoms manifest and patients seek medical help, approximately 70% are already in advanced stages. Furthermore, distinguishing between benign and malignant tissue types is particularly challenging. During exploratory laparotomy for OC, it is observed that only a small percentage of tumors are confined to the ovaries; the majority have already metastasized to the bilateral adnexa, greater omentum, and other pelvic organs. Consequently, OC presents substantial challenges in both diagnosis and treatment. Due to the difficulty of early detection, most clinical samples come from patients with stage III or IV OC, with very few at an early stage. To enhance early diagnosis, we will continue to collect clinical samples and related follow-up data from early-stage OC patients in future studies.

## Conclusion

This study is the first identification of diagnostic biomarkers from plasma EV metabolites in OC patients using machine learning algorithms. The profile of ovarian EV metabolites was characterized by metabolites associated with the metabolism of carbohydrates, amino acids, and lipids. We demonstrated that the RF Model, combined with sensitive thermal separation probe-based mass spectrometry analysis of plasma EVs, can effectively identify OC patients with high accuracy. Thus, our study has shortlisted a set of potential biomarkers in plasma EVs, and the proposed approach could serve as a routine prescreening tool for OC.

## Supplementary Information

The online version contains supplementary material available at https://doi.org/10.1186/s13048-025-01590-w.

Supplementary Material 1.
Supplementary Material 2.
Supplementary Material 3.
Supplementary Material 4.
Supplementary Material 5.
Supplementary Material 6.
Supplementary Material 7.
Supplementary Material 8.

**Acknowledgements**
We thank all collaborators for data collection. We also thank all the study participants.

**Authors' contributions**
FL contributed to the sample and data collection, XP, and XW performed the statistical analysis, interpreted the results, and wrote the manuscript. DM contributed to data collection and interpreting the results, SG and JS contributed to interpreting the results and wrote the manuscript. XZ, RR, LW and ZC contributed to the samples collection. RC commented on the experimental design and revised the manuscript. T-LH and YY devised the original laboratory study. T-LH interpreted the results, supported the writing of the manuscript, directed the project, guarantor of this work and, as such, had full access to all the data in the study and takes responsibility for the integrity of the data and the accuracy of the data analysis. All authors contributed to the article and approved the submitted version.

**Funding**
This study was supported by the Foundation of State Key Laboratory of Ultrasound in Medicine and Engineering (2023KFKT002), Chongqing Science & Technology Commission (cstc2021jcyj-msxmX0213), Chongqing Municipal Education Commission (KJZD-K202100407), the Senior Medical Talents

Program of Chongqing for Young and Middle-aged [2022] 15, the Kuanren Talents Program of the Second Affiliated Hospital of Chongqing Medical University, and Beijing Natural Science Foundation (No. 1S24091).

### Data availability
No datasets were generated or analysed during the current study.

## Declarations

### Ethics approval and consent to participate
Research Ethics Committee of the Second Affiliated Hospital of Chongqing Medical University approved the study (202164).

### Consent for publication
Not applicable.

### Competing interests
The authors declare no competing interests.

### Author details
[1]Department of Obstetrics and Gynaecology, The Second Affiliated Hospital of Chongqing Medical University, Chongqing, China. [2]State Key Laboratory of Ultrasound in Medicine and Engineering, College of Biomedical Engineering, Chongqing Medical University, Chongqing, China. [3]Chongqing Key Laboratory of Biomedical Engineering, Chongqing Medical University, Chongqing, China. [4]Department of Reproductive Center, The First Affiliated Hospital of Chongqing, Medical University, Chongqing, China. [5]Department of Obstetrics and Gynecology, Second Affiliated HospitalArmy Medical University, Chongqing, China. [6]Department of Obstetrics, The First Affiliated Hospital of Chongqing Medical University, Chongqing, China. [7]Department of Oral Sciences, Faculty of Dentistry, Sir John Walsh Research Institute, University of Otago, Dunedin, New Zealand.

Received: 7 May 2024 Accepted: 6 January 2025
Published online: 12 February 2025

### References
1. Arneth, B. (2019). Tumor Microenvironment. Medicina 56(1). https://doi.org/10.3390/medicina56010015.
2. Bachmayr-Heyda A, Aust S, Auer K, Meier SM, Schmetterer KG, Dekan S, Gerner C, Pils D. Integrative Systemic and Local Metabolomics with Impact on Survival in High-Grade Serous Ovarian Cancer. Clin Cancer Res. 2017;23(8):2081–92. https://doi.org/10.1158/1078-0432.CCR-16-1647.
3. Bachurski D, Schuldner M, Nguyen PH, Malz A, Reiners KS, Grenzi PC, et al. Extracellular vesicle measurements with nanoparticle tracking analysis - An accuracy and repeatability comparison between NanoSight NS300 and ZetaView. J Extracell Vesicles. 2019;8(1):1596016. https://doi.org/10.1080/20013078.2019.1596016. PMID: 30988894; PMCID: PMC6450530.
4. Bray F, Ferlay J, Soerjomataram I, Siegel RL, Torre LA, Jemal A. Global cancer statistics 2018: GLOBOCAN estimates of incidence and mortality worldwide for 36 cancers in 185 countries. Ca-a Cancer J Clin. 2018;68(6):394–424. https://doi.org/10.3322/caac.21492.
5. Brett MR, Brett MR, Jennifer BP, Thomas AS, Jennifer BP, Thomas AS. Epidemiology of ovarian cancer: a review. Cancer Biol Med. 2017;14(1):9–32. https://doi.org/10.20892/j.issn.2095-3941.2016.0084.
6. Chang L, Ni J, Zhu Y, Pang B, Graham P, Zhang H, et al. Liquid biopsy in ovarian cancer: recent advances in circulating extracellular vesicle detection for early diagnosis and monitoring progression. Theranostics. 2019;9(14):4130–40. https://doi.org/10.7150/thno.34692.
7. Cocucci E, Meldolesi J. Ectosomes and EVs: shedding the confusion between extracellular vesicles. Trends Cell Biol. 2015;25(6):364–72. https://doi.org/10.1016/j.tcb.2015.01.004.
8. Denkert C, Budczies J, Kind T, Weichert W, Tablack P, Sehouli J, et al. Mass spectrometry-based metabolic profiling reveals different metabolite patterns in invasive ovarian carcinomas and ovarian borderline tumors. Can Res. 2006;66(22):10795–804. https://doi.org/10.1158/0008-5472.Can-06-0755.
9. Gamcsik MP, Kasibhatla MS, Teeter SD, Colvin OM. Glutathione levels in human tumors. Biomarkers. 2012;17(8):671–91. https://doi.org/10.3109/1354750x.2012.715672.
10. Gowda GA, Djukovic D. Overview of mass spectrometry-based metabolomics: opportunities and challenges. Methods Mol Biol. 2014;1198:3–12. https://doi.org/10.1007/978-1-4939-1258-2_1.
11. Han TL, Cannon RD, Gallo SM, Villas-Bôas SG. A metabolomic study of the effect of Candida albicans glutamate dehydrogenase deletion on growth and morphogenesis. NPJ Biofilms Microbiomes. 2019;5(1). https://doi.org/10.1038/s41522-019-0086-5.
12. Huang ZZ, Chen C, Zeng Z, Yang H, Oh J, Chen L, Lu SC. Mechanism and significance of increased glutathione level in human hepatocellular carcinoma and liver regeneration. FASEB J. 2001;15(1):19–21. https://doi.org/10.1096/fj.00-0445fje.
13. Iddamalgoda L, Das PS, Aponso A, Sundararajan VS, Suravajhala P, Valadi JK. Data Mining and Pattern Recognition Models for Identifying Inherited Diseases: Challenges and Implications. Front Genetics. 2016;7. https://doi.org/10.3389/fgene.2016.00136.
14. Li Wei. The investigation on anti-tumor and hepatoprotective effects of 5-HMF and Maltol. The Chinese Academy of Agricultural Sciences. 2015. https://doi.org/10.27630/d.cnki.gznky.2015.000003.
15. Liu M, Liu Y, Feng H, Jing Y, Zhao S, Yang S, Zhang N, Jin S, Li Y, Weng M, Xue X, Wang F, Yang Y, Jin X, Kong D. Clinical Significance of Screening Differential Metabolites in Ovarian Cancer Tissue and Ascites by LC/MS. Front Pharmacol. 2021;12:701487. https://doi.org/10.3389/fphar.2021.701487.
16. Luo, P., Mao, K., Xu, J., Wu, F., Wang, X., Wang, S., et al. Metabolic characteristics of large and small extracellular vesicles from pleural effusion reveal biomarker candidates for the diagnosis of tuberculosis and malignancy. J Extracell Vesicles. 2020;9(1). https://doi.org/10.1080/20013078.2020.1790158.
17. Magdalena Derbis MS. EVs in plasma of patients with ovarian carcinoma: potential biomarkers of tumor progression and response to therapy. Gynecol Obstet. 2012;s4. https://doi.org/10.4172/2161-0932.S4-003.
18. Mashouri L, Yousefi H, Aref AR, Ahadi Am, Molaei F, Alahari SK. EVs: composition, biogenesis, and mechanisms in cancer metastasis and drug resistance. Mol Cancer. 2019;18(1). https://doi.org/10.1186/s12943-019-0991-5.
19. Mastrangelo A, Ferrarini A, Rey-Stolle F, García A, Barbas C. From sample treatment to biomarker discovery: A tutorial for untargeted metabolomics based on GC-(EI)-Q-MS. Anal Chim Acta. 2015;900:21–35. https://doi.org/10.1016/j.aca.2015.10.001.
20. Menay F, Herschlik L, De Toro J, Cocozza F, Tsacalian R, Gravisaco MJ, et al. EVs Isolated from Ascites of T-Cell Lymphoma-Bearing Mice Expressing Surface CD24 and HSP-90 Induce a Tumor-Specific Immune Response. Front Immunol. 2017;8. https://doi.org/10.3389/fimmu.2017.00286.
21. Mohamed AS, Hosney M, Bassiony H, Hassanein SS, Soliman, AM, Fahmy SR, et al. Sodium pentobarbital dosages for exsanguination affect biochemical, molecular and histological measurements in rats. Sci Rep.2020;10(1). https://doi.org/10.1038/s41598-019-57252-7.
22. Poojary MM, Passamonti P. Improved conventional and microwave-assisted silylation protocols for simultaneous gas chromatographic determination of tocopherols and sterols: method development and multi-response optimization. J Chromatogr A. 2016;1476:88–104. https://doi.org/10.1016/j.chroma.2016.10.064.
23. Roy D, Pascher A, Juratli MA, Sporn JC. The Potential of Aptamer-Mediated Liquid Biopsy for Early Detection of Cancer. Int J Mol Sci. 2021;22(11). https://doi.org/10.3390/ijms22115601.
24. Spencer PS, Kisby GE. Role of hydrazine-related chemicals in cancer and neurodegenerative disease. Chem Res Toxicol. 2021;34(9):1953–69. https://doi.org/10.1021/acs.chemrestox.1c00150.
25. Stewart C, Ralyea C, Lockwood S. Ovarian cancer: an integrated review. Semin Oncol Nurs. 2019;35(2):151–6. https://doi.org/10.1016/j.soncn.2019.02.001.
26. Teruel-Montoya R, Luengo-Gil G., Vallejo, F., Yuste, J.E., Bohdan, N., García-Barberá, N., et al. Differential miRNA expression profile and proteome in plasma EVs from patients with paroxysmal nocturnal hemoglobinuria. Sci Rep. 2019;9(1). https://doi.org/10.1038/s41598-019-40453-5.
27. Wu Z, Zhu M, Kang Y, Leung ELH, Lei T, Shen C, et al. Do we need different machine learning algorithms for QSAR modeling? A comprehensive assessment of 16 machine learning algorithms on 14 QSAR data sets. Briefings Bioinformatics. 2021;22(4). https://doi.org/10.1093/bib/bbaa321.

28. Xia Y, Rao L, Yao H, Wang Z, Ning P, Chen X. Engineering macrophages for cancer immunotherapy and drug delivery. Adv Mater. 2020;32(40). https://doi.org/10.1002/adma.202002054.
29. Zhong X, Ran R, Gao S, Shi M, Shi X, Long F, et al. Complex metabolic interactions between ovary, plasma, urine, and hair in ovarian cancer. Front Oncol. 2022;12. https://doi.org/10.3389/fonc.2022.916375.

## Publisher's Note